PAPER • OPEN ACCESS

Handling Individual Pitch Control within an Actuator Disk framework: verification against the Actuator Line method and application to wake interaction problems

To cite this article: M. Moens *et al* 2022 *J. Phys.: Conf. Ser.* **2265** 022053

Journal of Physics: Conference Series **2265** (2022) 022053 doi:10.1088/1742-6596/2265/2/022053

Handling Individual Pitch Control within an Actuator Disk framework: verification against the Actuator Line method and application to wake interaction problems

M. Moens[1]**, M. Coquelet**[1,2]**, F. Trigaux**[1] **, P. Chatelain**[1]

[1]Institute of Mechanics, Materials and Civil engineering, Université catholique de Louvain, 1348 Louvain-la-Neuve, Belgium

[2]Fluids-Machines Department, Université de Mons, 7000 Mons, Belgium.

E-mail: `maud.moens@uclouvain.be`

Abstract. The present study aims at assessing the Actuator Disk (AD) method supplemented with an Individual Pitch Control (IPC) strategy, at a resolution appropriate for the Large Eddy Simulation of large wind farms. The IPC scheme is based on a state-of-the art individual pitch control, generalized to be applied to an AD approach. This procedure also requires an accurate recovery of the flapwise bending moment on each blade, which is not trivial for a disk-type model. In order to compute flapwise moments on each blade, blade trajectories are reproduced through the disk and the AD aerodynamic forces are interpolated onto these virtual blades at each time step. We verify the AD model with IPC in simulations of an isolated wind turbine, for different wind speeds and turbulence intensities, and in a configuration with two rotors. We compare the AD statistics with those obtained using an Actuator Line (AL) method. The comparison done in terms of equivalent moment shows that the AD and AL simulations produce very similar results.

1. Introduction

Fatigue damage is a critical factor in the lifetime of a wind turbine and its reduction gains an increasing importance due to the trend towards larger wind turbines. Individual Pitch Control (IPC) plays a key role in compensating loads. Collective pitch control adjusts the pitch angle of all the blades to the same value at the same time. In contrast, IPC dynamically and individually adjusts the pitch of each blade, which leads to a reduction of fatigue loads on the wind turbine components. In recent years, two different IPC techniques have been developed, characterized by the type of loads they aim at attenuating. In the first approach, the IPC strategy is based on a single-blade control [1] or a Clarke transform-based control [2], in order to reduce the unsteady loads on the rotating blades. In the second technique, the Coleman transform is used, targeting load reductions in the non-rotating turbine structures [3]. Lio *et al.* [4] demonstrated that, despite of their different architectures, those two techniques lead to very similar performances in terms of load reductions on fixed and rotating wind turbine components.

Numerical approaches offer a convenient framework for investigating IPC strategies. The highest fidelity tools that also capture the wake response usually consider Large Eddy Simulation

(LES), combined to discrete type line approaches [5, 6], such as the Actuator Line (AL) or Lifting Line methods. The use of these wind turbine models remains computationally affordable at the scale of a small wind farm. When IPC strategies will be considered at larger wind farm scales, for individual load alleviation or global wind farm control, the resolution required by the AL method will become prohibitive, and the Actuator Disk (AD) method should be used as it suits coarser spatio-temporal resolutions. It is not trivial to transpose IPC strategies to a disk-type approach as this fundamentally considers blade averaged effects. However, the most advanced AD approaches implies a discretization in both radial and azimuthal directions [7, 8, 9]; this last feature allows the AD model to capture temporal and spatial variations in the rotor loads, which could give relevant information about the loading on a blade that crosses the disk surface.

To the authors' knowledge, a thorough verification of the capture of IPC schemes by an AD approach has not been performed, and this work aims at filling this gap in the literature. In particular, we here want to assess an AD approach with IPC at a resolution appropriate for wind farm simulations. We consider an advanced AD method, such as the ones described previously. As the Coleman transformation is the most widely used and leads to similar performances as other techniques [4], we choose this approach for the IPC scheme, and we generalize it to be applied to an AD model. This procedure also requires an accurate recovery of the flapwise bending moment on each blade and we here choose the procedure described in [10] and that proposes to replicate blade trajectories through the disk and to interpolate the AD aerodynamic forces onto these virtual blades at each time step. We verify the AD approach in both freestream and waked configurations, by comparing its behavior to that an AL method at a finer resolution. We also perform AD simulations at a finer resolution in order to highlight possible resolution effects.

The flow solver, the wind turbine modeling, the estimation of the fatigue loads and the IPC scheme are described in Section 2. Section 3 presents simulations of an isolated wind turbine, in different wind speeds and turbulence intensities, while simulations with two-aligned rotors are presented in Section 4. Finally, our conclusions are drawn in Section 5.

2. Methodology

2.1. Flow Solver

We consider the Large Eddy Simulation (LES) of incompressible flows. It is performed using an in-house fourth-order finite difference (FD4) code [11], formulated in primitive variables (i.e. in velocity and pressure) and using a staggered mesh arrangement. Details about the code, the main equations and the subgrid scale model can be found in Moens *et al.* [9]. Although the FD4 code can handle an accurate Atmospheric Boundary Layer representation, we will here consider a more simplified representation of the rotor environment, i.e. a prescribed wind shear at the inflow, over which turbulent fluctuations are imposed (discussed in Section 3). This allows us to have a better controllability of the inflow characteristics and to reproduce the same inflow structures, whatever the resolution of the simulation.

2.2. Wind turbine modeling

The wind turbine is added through external body force terms acting on the flow. In the present study, we consider two wind turbine models: an Actuator Disk (AD) method and an Actuator Line (AL) approach.

We here choose an AD method including torque effects and force computations based on the prevailing velocities at the disk location, and supplemented with a tip-loss correction [9]. The AD procedure implies a discretization in both radial and azimuthal directions; this last feature allows the wind turbine model to capture temporal and spatial variations in the rotor loads, which could give relevant information about blade loading and bending moments. The methodology for estimating the blade fatigue loads is detailed in Section 2.3.

The AL approach [12, 13] is used to verify the IPC applied to an AD model: the forces are mollified using a 2D non-uniform Gaussian kernel, which avoids spanwise mollification and hence produces a consistent tip behavior without requiring any additional correction.

Aeroelastic effects are not taken into account, and the blades thus act as rigid bodies in both AD and AL methods. The effects of the tower shadow on blade aerodynamics are also not taken into account. However, the presence of the tower may have a significant impact in terms of periodic variations of the blade loads. One way to mimic the effect of the tower is to use a virtual force, similarly to the AL approach [14, 15, 16, 17]. Adding the tower shadow in such a way would require further investigations about the impact of the coarse LES resolution on the tower modeling. A higher fidelity approach consists in using immersed boundary methods [18]. However, this increases the level of complexity and it is thus computationally more expensive, and again, the impact of the resolution should be investigated. A lower fidelity method would consist in adding a correction that accounts for the tower influence on the velocity field at the rotor level (e.g, the approach used in AeroDyn, the aerodynamic module of FAST, and based on the work of Bak *et al.* [19]). Again, the implementation of such a model in the AD approach should be further investigated and verified.

2.3. Estimation of the blade loads

IPC and the estimation of fatigue damages require to recover the flapwise root bending moment on each blade. The flapwise moment per blade b is denoted $M_{f,b}$ and is evaluated based on the aerodynamic contributions only

$$M_{f,b} = \int_{R_{hub}}^{R_{tip}} (r - R_{hub})\, \mathbf{F_b}.\mathbf{e_n}\, dr \; , \tag{1}$$

where r is the local radius; R_{hub} and R_{tip} are the hub and tip radii, respectively; $\mathbf{F_b}$ is the aerodynamic blade forces per blade length element dr; $\mathbf{e_n}$ is the unit vector normal to the rotor plane.

For discrete line type approaches, such as the AL method, the instantaneous blade loading is directly available and can be integrated along the blade span. For the AD method, we propose to replicate the blade trajectories through the disk and recompute blade-attached aerodynamic forces. At each particular radial position, r, and time, t, the forces acting on the blade b, $\mathbf{F_b}$, are thus interpolated from the AD forces of the two adjacent disk elements at the same radius r (see Moens et al. [10] for more details about this approach). The fatigue loads estimated using this methodology are in excellent agreement with those obtained using a Vortex Particle-Mesh method coupled to immersed Lifting Lines [10]. For the present study, we note that the flapwise moments presented for the AD method are all computed based on this methodology. This flapwise moment estimation can be performed online in the AD simulations, avoiding additional post-processing computations and allowing its integration in the IPC scheme.

2.4. Individual Pitch Control

The AD and AL methods are supplemented with classical torque and collective blade pitch controllers. In this work, an IPC strategy is moreover implemented. In a first approach, we add a state-of-the-art individual pitch controller, initially proposed by Bossanyi [3], and that is based on the Coleman transform: we denote this methodology as CT-IPC. In a classical discrete blade type approach, the CT-IPC implies a projection of the loads expressed in the rotating coordinate frame of the blades on the vertical and lateral directions: the flapwise bending moments of the three blades $M_{f,1}(t)$, $M_{f,2}(t)$ and $M_{f,3}(t)$ are projected on a tilting moment, $M_t(t)$ and a yawing one $M_y(t)$ using the inverse Coleman transform (Eq. 2, with $\theta_1(t)$, $\theta_2(t)$ and $\theta_3(t)$ being the azimuthal blade positions). The values $\beta_t(t)$ and $\beta_y(t)$ that bring $M_t(t)$ and $M_y(t)$

to 0 are determined using a Proportional-Integral (PI) controller, and are finally projected on the blades by means of the Coleman transform (see Eq 3). The individual pitch actions $\beta_1(t)$, $\beta_2(t)$ and $\beta_3(t)$ are then added to the collective blade pitch angle.

$$\begin{pmatrix} M_t(t) \\ M_y(t) \end{pmatrix} = \begin{pmatrix} \frac{2}{3}\cos(\theta_1(t)) & \frac{2}{3}\cos(\theta_2(t)) & \frac{2}{3}\cos(\theta_3(t)) \\ \frac{2}{3}\sin(\theta_1(t)) & \frac{2}{3}\sin(\theta_2(t)) & \frac{2}{3}\sin(\theta_3(t)) \end{pmatrix} \begin{pmatrix} M_{f,1}(t) \\ M_{f,2}(t) \\ M_{f,3}(t) \end{pmatrix} \quad (2)$$

$$\begin{pmatrix} \beta_1(t) \\ \beta_2(t) \\ \beta_3(t) \end{pmatrix} = \begin{pmatrix} \cos(\theta_1(t)) & \sin(\theta_1(t)) \\ \cos(\theta_2(t)) & \sin(\theta_2(t)) \\ \cos(\theta_3(t)) & \sin(\theta_3(t)) \end{pmatrix} \begin{pmatrix} \beta_t(t) \\ \beta_y(t) \end{pmatrix} \quad (3)$$

For the AL method, it is trivial to compute the flapwise moments and apply individual blade pitch actions. For the AD approach, the procedure described in Section 2.3 is used for estimating the flapwise bending moments on the three blades. The inverse Coleman transform of Eq. 2 and the PI controller are used to compute $\beta_t(t)$ and $\beta_y(t)$, as in the methodology described in the previous paragraph. $\theta_1(t)$, $\theta_2(t)$ and $\theta_3(t)$ of Eq. 2 thus represent the position of the artificial blades. For projecting $\beta_t(t)$ and $\beta_y(t)$ on the disk elements, we use the Coleman transform generalized for the n elements of the AD in the azimuthal direction, with $\theta_{AD,1}, \ldots, \theta_{AD,n}$, the azimuthal position of the AD elements

$$\begin{pmatrix} \beta_1(t) \\ \vdots \\ \beta_n(t) \end{pmatrix} = \begin{pmatrix} \cos(\theta_{AD,1}) & \sin(\theta_{AD,1}) \\ \vdots & \vdots \\ \cos(\theta_{AD,n}) & \sin(\theta_{AD,n}) \end{pmatrix} \begin{pmatrix} \beta_t(t) \\ \beta_y(t) \end{pmatrix} \quad (4)$$

The collective blade pitch angle is added to $\beta_1, \ldots, \beta_n$, and those values are used in the computation of the aerodynamic forces of the AD elements.

We note that, theoretically, the Coleman transform should decouple the blade load signals in a yaw-axis and tilt-axis, allowing the use of a simple single-input-single-output controller, one per axis. However, in practice, the transform system may still show coupling between the axes [20, 21], requiring more advanced multivariable control architectures [21] or including of an azimuth offset in the reverse Coleman transform [22]. We let the implementation of more complex control schemes for further investigations, mainly when more dynamic systems (larger rotor, flexible blades) will be considered.

3. Simulations of an isolated wind turbine

3.1. Configuration

We first aim at assessing the fatigue loads and their potential reduction with IPC in a AD approach for an isolated wind turbine. We here consider the “NREL offshore 5-MW baseline wind turbine” [23], denoted NREL-5MW in the remainder of this paper. The domain size is $12D \times 4D \times 4D$, where D is the rotor diameter ($D = 126$ m for the NREL-5MW), and the wind turbine is located at $(3D, H_{hub}, 2D)$. H_{hub} is the hub height of the NREL-5MW and is equal to 90 m [23]. AL simulations are performed using a resolution of 64 points per D, while the AD simulations are performed at two particular resolutions: 16 and 64 points per D. The first one is used to assess the performances of the AD model at a resolution appropriate for efficient but still accurate wind farm simulations; the second one is used to highlight possible resolution effects.

We consider a rotor impacted by a wind shear, defined using the classical power law:

$$\frac{U(y)}{U_{hub}} = \left(\frac{y}{H_{hub}}\right)^{\alpha} \quad (5)$$

where y the vertical elevation from the ground; $U(y)$ the streamwise velocity profile imposed as the inlet section; U_{hub} the streamwise velocity at hub height; and α the shear coefficient. α is set to 0.2: this value is chosen in order to have an important shear, which will generate large 1P oscillations on the turbine blade loads, and will highlight the contribution of the IPC and the possible differences existing between the AD and the AL approaches. We consider two particular operating conditions: during the optimum operating condition ($U_{hub} = 9$ m/s) and during the rated operation ($U_{hub} = 15$ m/s).

For each wind speed, four level of turbulence intensities (TIs) at hub height are investigated: 0, 6, 10 and 14%. The turbulence field is generated using the Mann algorithm [24] and is added to the shear inflow. In order to compare the unsteady loads and the action of the IPC, it is important that the same turbulent structures impact the wind turbine at the same times. Only one synthetic turbulence box is thus generated per wind speed and per TI, and the resolution of the turbulent field is adapted to the considered resolution (16 points or 64 points per D). All the statistics presented in this section are computed or accumulated over one turbulence box period, T_{Mann} and over the three blades. T_{Mann} is set to be about 10 minutes for both U_{hub}. In order to highlight the impact of the IPC, all the simulations are also performed using classical control only, i.e. collective blade pitch and torque controls. This control case is denoted CPC in the remainder of this paper.

3.2. Flapwise moment history

An example of the history of the flapwise root bending moment for one blade is reported on Fig. 1, for the AD and AL approaches. The results are shown for $U_{hub} = 15$ m/s and TI = 6%, and for a small time period of 20 seconds. First of all, for both AL and AD methods, Fig. 1 highlights the positive impact of the CT-IPC. Compared to the signals obtained using CPC, the amplitude of the oscillations related to the blade passage in the wind shear decreases considerably; this will also be highlighted in the resulting equivalent moment (see Section 3.5). We also see that, either with or without IPC, the AD method at the finest resolution produces a flapwise moment that is very close to that obtained using the AL approach. This clearly highlights the potential of using an AD method with IPC strategies. If we compare the AD at a coarser resolution with the other results, we observe small discrepancies: the AD method at a coarser resolution cannot capture the high frequency oscillations and thus presents a smoother signal. The response of the collective blade pitch and torque control schemes may also be slightly different. However, the $M_{f,1}$ history remains close to the results obtained at a finer resolution.

We chose this particular velocity for the example because the rotor operates above rated conditions and has a near-constant rotor speed (12.1 RPM for the NREL-5MW). This allows the AL and the AD methods to have the exact same blade trajectory, leading to a consistent comparison of the instantaneous signals. For $U_{hub} = 9$ m/s, the rotor speed varies a lot over T_{Mann} as the rotor operates below rated condition. As the aerodynamic forces may be slightly different according to the wind turbine model and the resolution (discussed in the next paragraph), the response of the controller varies, bringing different rotor speed histories and making the comparison uneasy. It is thus more consistent to investigate the variables of interest as spectra, time-averaged values or equivalent moments.

3.3. Power spectral densities

Fig. 2 presents the one-sided power spectral densities (PSD) of M_f for $U_{hub} = 9$ and 15 m/s and TI = 6%. Again, the results for both CPC and CT-IPC are reported. Globally, for each control case and U_{hub}, there is a very good agreement between all the approaches over a broad band at low frequencies. For higher frequencies, the PSD of M_f obtained using the AD method at a coarse resolution drops beyond a certain cut-off frequency. Figs. 2(a) and 2(b) also highlight the impact of the CT-IPC, with a peak that is attenuated at the rotation frequency.

Journal of Physics: Conference Series **2265** (2022) 022053 doi:10.1088/1742-6596/2265/2/022053

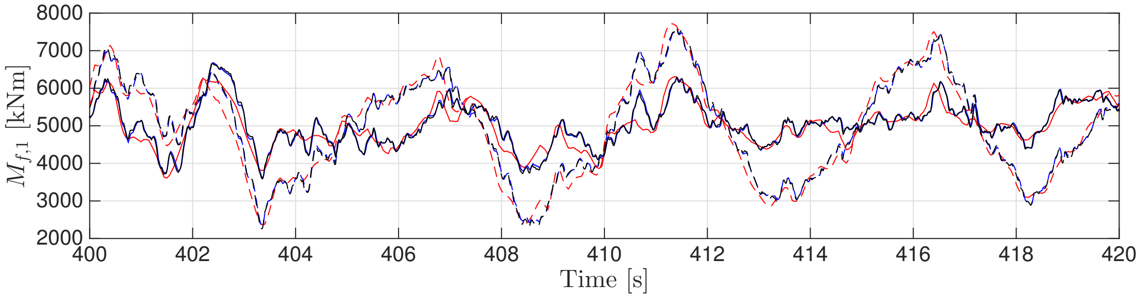

Figure 1. $U_{hub} = 15$ m/s and $TI = 6\%$: history of $M_{f,1}$ for the AD approach at a coarse resolution (red lines) and at a fine resolution (blue lines) and for the AL method (black lines). The dashed and solid lines represent simulations with CPC and CT-IPC, respectively.

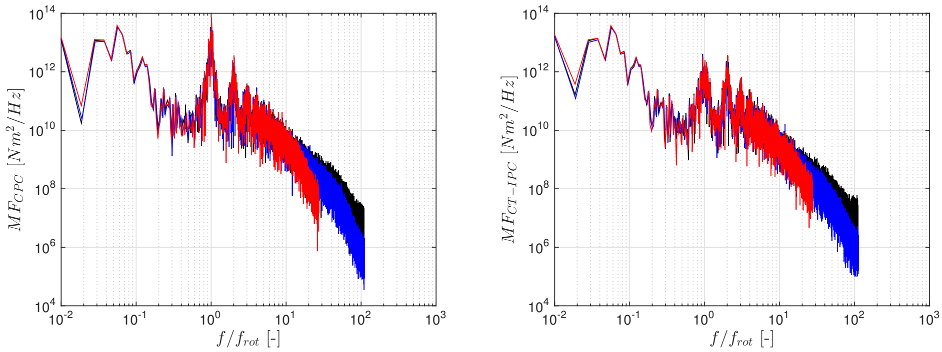

(a) $U_{hub} = 9$ m/s and $TI = 6\%$

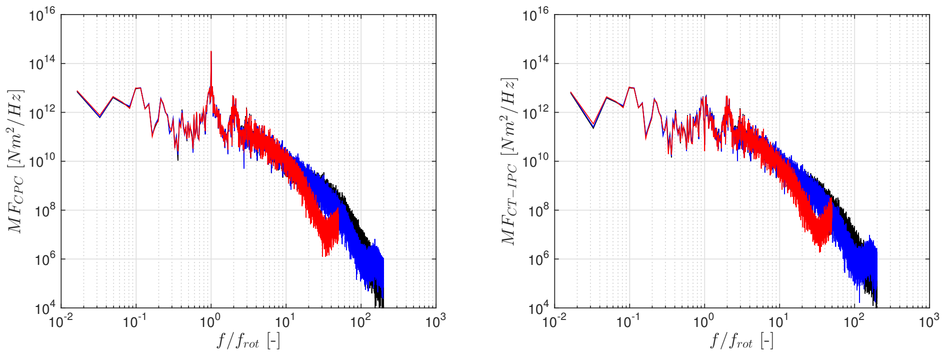

(b) $U_{hub} = 15$ m/s and $TI = 6\%$

Figure 2. PSD of M_f for the AD approach at a coarse resolution (red lines) and at a fine resolution (blue lines) and for the AL method (black lines). CPC and CT-IPC results are presented on the left and on the right of each subfigure, respectively. f_{rot} is the rotation frequency.

3.4. Time-averaged statistics

We continue our comparison by investigating the time-averaged flapwise root bending moments and mechanical powers (see Fig. 3): we reported the AD results over the ones obtained using the AL approach (we consider that the AL approach is our reference).

Globally, we see that $U_{hub} = 9$ m/s leads to more discrepancies between the AD and the AL results. The AD approach simulated at a coarser resolution leads to ratios slightly higher

Journal of Physics: Conference Series **2265** (2022) 022053 doi:10.1088/1742-6596/2265/2/022053

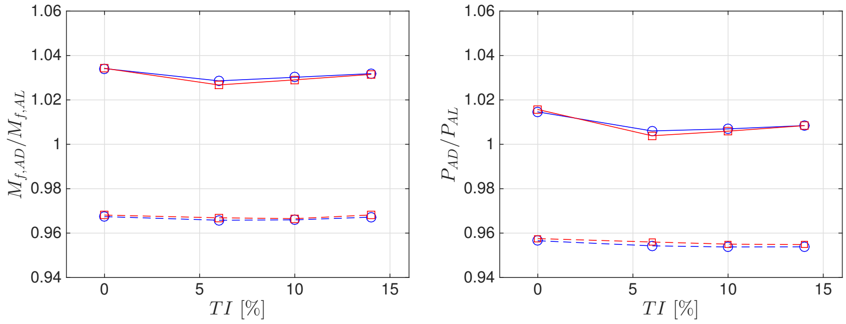

(a) U_{hub} = 9 m/s

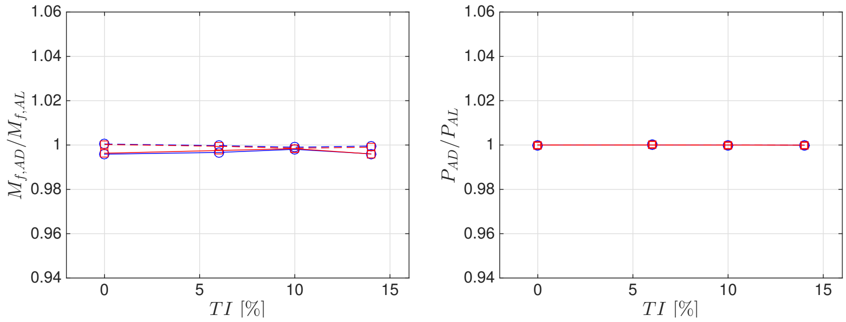

(b) U_{hub} = 15 m/s

Figure 3. Ratios of the time-averaged M_f and power P obtained using the AD approach over those computed using the AL method. The results are shown for the AD method at a coarse resolution (solid line) and at a fine resolution (dashed line). CPC : blue line with circles; CT-IPC : red line with squares.

than one. It is probably due to the loading distribution on the blade, which is high near the blade tip at this particular operating condition [9]. Indeed, potential loading differences in the tip region may have a significant impact in M_f and P due to the presence of the local radius in their computation. Even supplemented with the tip-loss correction, the AD method misses the decrease in the normal and tangential forces, which increases the discrepancies with the AL method. Conversely, at a finer resolution, the AD method better captures the tip effect and the contribution of the tip-loss factor may be too large, as shown in [9]. This could explain the ratios slightly lower than one in Fig. 3(a). We also cannot exclude an effect of resolution in the AL method, which also misses some tip effects. Performing simulations at a finer resolution should allow the AL to better capture the tip effect, and being closer to the one obtained using a disk with its tip-loss correction. The controller response may also be different, potentially increasing the discrepancies.

For U_{hub} = 15 m/s, the AD method in both resolutions leads to results that are very close to those obtained using the AL approach. This can be explained in several manners: first, at this operating condition, the blade loading is more concentrated on the inboard part [9], mitigating the potentiel differences in terms of the blade tip behavior discussed above. The rotor also operates at a low thrust coefficient, decreasing differences occurring between a discrete line type approach and a disk approach [9]. Finally, at this wind speed, the controller aims at conserving the rated power exactly and it is thus logical to have power ratios that are equal to one in Fig. 3(b). We also observe that the results obtained using CT-IPC are similar to those obtained using CPC: CT-IPC does not contribute to further increase or decrease the differences between the wind turbine models.

3.5. Equivalent moments

In order to verify the impact of the CT-IPC on the fatigue damage in both AD and AL methods, a quantitative fatigue indicator, the equivalent moment M_{eq}, is computed. M_{eq} is estimated based on a rainflow counting (RFC) method [25] combined with a Palmgren-Miner rule [26].

Assuming that the moment is proportional to the stress, M_{eq} is equal to $\left(\sum_{i=1}^{L_c} \frac{n_i M_i^m}{N_{eq}}\right)^{\frac{1}{m}}$, where i and L_c represent the load case number and the total number of load cases, respectively; n_i is the number of cycles for the particular moment amplitude M_i and determined using the RFC; m is a parameter dependent on the material ($m = 10$ for blades made of fiberglass [27], as for the NREL-5MW); N_{eq} is an arbitrary number of cycles. As we will always investigate M_{eq} as ratios, N_{eq} does not need to be defined in this work.

We first compare the equivalent moments obtained using the AD approach with those obtained using the AL method. The ratios are reported in Figs. 4(a)(left) and 4(b)(left).

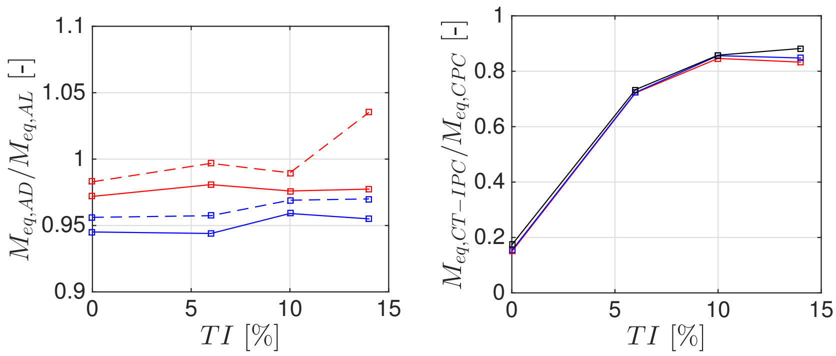

(a) $U_{hub} = 9$ m/s

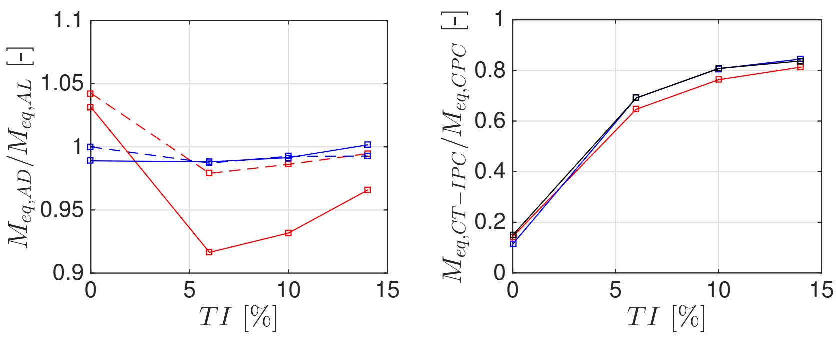

(b) $U_{hub} = 15$ m/s

Figure 4. Left of each subfigure : Ratio of the AD flapwise equivalent moments, over the AL ones, for the AD method at a coarse resolution (red line) and at a fine resolution (blue line). CPC : solid line; CT-IPC : dashed line. Right of each subfigure: Ratio of the flapwise equivalent moments obtained using CPC and CT-IPC, for AD methods at a coarse resolution (red line), at a fine resolution (blue line) and AL approach (black line) methods.

Globally, the differences are small and remains of the same order of magnitude as those observed in terms of time-averaged M_f. However, for $U_{hub} = 15$ m/s, the differences obtained using CT-IPC at a coarse resolution are higher. This can be explained by analysing the number of cycles as a function of the moment amplitude, for the particular case $U_{hub} = 15$ m/s and TI=6% (Fig. 5). The behavior for the other turbulence intensities is similar, and the following explanations remain valid. Although the cycle distribution is very similar in both approaches, we observe some discrepancies. First, as expected, for both CT-CPC and IPC, the AD procedure presents lower n_i at small moment amplitudes, due to its coarse resolution. However, these relatively large differences do not strongly impact the fatigue damage estimate. It is partly due to the presence of the m-exponent (of a value of 10 in our study) that rather reinforces the contribution of the large moment amplitudes to M_{eq} [28, 10].

Regarding these cycles of large amplitude, their distribution is marginally captured by the simulations as their number can be just one or even a half. In the case of CT-IPC, we see that the AL approach captures cycles of large moment amplitude that the AD method does not capture: even if the number of those cycles is lower than one, it significantly contributes to the equivalent moment and increases the differences with the AD method. This explains the largest differences observed in Fig. 4. In order to fill those scales and having n_i considerably higher than one, and thus more consistent comparisons, more simulations with different turbulence realizations and a same TI should be performed or T_{Mann} should be increased. However, this would considerably increase the computational costs, mainly for the high resolution simulations. Fig. 5 also clearly highlights the effect of the CT-IPC, with a peak in the medium amplitudes that is clearly attenuated, and a cycle distribution moved to the smaller moment amplitudes.

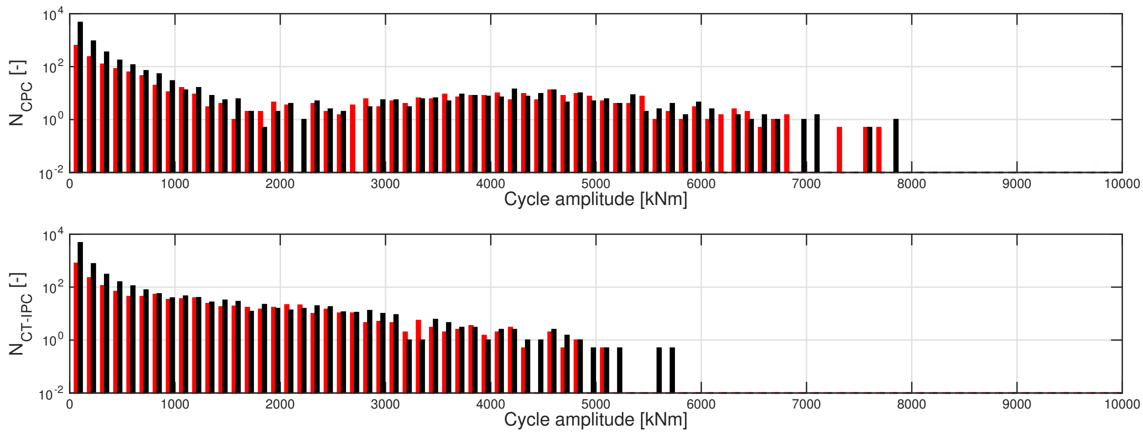

Figure 5. U_{hub} = 15 m/s and TI = 6% : Number of cycles for M_f for the AD method at a coarse resolution (red bars) and the AL approach (black blars).

In Figs. 4(a)(right) and 4(b)(right), the ratio between the equivalent moments obtained using the CT-IPC and CPC are shown for the AD and the AL methods. Globally, the ratios for the AD and the AL methods are very close to each other, although the discrepancies slightly increase with the TI. However, the differences remain small, with a maximum of 4%.

4. Simulations of two rotors

4.1. Configuration

We now assess the IPC used within an AD framework in a waked configuration. We consider two turbines, denoted WT_1 and WT_2, separated by 6D in a domain of size $14D \times 4D \times 4D$. The positions of WT_1 and WT_2 are $(3D, H_{hub}, 2D)$ and $(9D, H_{hub}, 2D)$, respectively. Again, the AL simulations are performed using a resolution of 64 points per D and the AD simulations are performed using two resolutions, 16 and 64 points per D. We still consider a sheared inflow, determined with Eq. 5, with α set to 0.2 for the same reason as above. In the present case, we want the turbine to operate at above rated wind speed. We also want to have a significant impact of the upstream turbine wake on the downstream rotor. This implies a strong wake deficit, and hence, a still high thrust coefficient and a limited wake recovery, implying a moderate TI. We therefore set U_{hub} of 12m/s and the hub TI of 6%. Again, the turbulence is generated using the Mann algorithm, using the same procedure as the one described in Section 3.1. However, in the present case, three turbulence boxes are generated, each one having a particular seed for the random number generator in the Mann algorithm: the statistics are then computed over the three turbulence seeds. This aims at having a better representation of the rarest events that may significantly contribute to the fatigue damages, as demonstrated in Section 3. Indeed, in this particular configuration, it is quite important, as the wake generated by the first wind turbine may have local variabilities according to the considered wind turbine model and/or the resolution, and thus a different impact on WT_2. In order to have consistent statistics and comparisons, it is important to increase the number of wind samples. Again, the statistics are accumulated over the three blades.

4.2. Equivalent moments

We first compare the equivalent moments produced by the AD methods with those obtained using the AL method. The ratios are reported in Fig. 6(a). The AD approach at a fine resolution produces results that are very close to those obtained using the AL method, with less than 1% of differences. The discrepancies slightly increase when we consider the AD at a coarser resolution. However, the differences remain small, with a maximum of less than 3%. This clearly confirms the potential of using IPC within an AD framework in wind farm simulations. The differences are also slightly smaller than the ones observed in Section 3, for the isolated wind turbine; this contributes to confirm that an increase in the number of wind samples would mitigate inconsistent effects due to the rarest events.

In Fig. 6(b), we highlight the fatigue load reduction obtained thanks to the CT-IPC, by reporting the ratios of the equivalent loads obtained using CT-IPC and CPC. If we compare the AD and AL results, we see that they produce ratios that are very similar, with a maximum error of 2%. We also note that the fatigue reduction is more significant for WT_1 (- 30%) than for WT_2 (about -8%). This behavior was already highlighted in the literature [6], and this is most likely due to the higher complexity of the flow impacting WT_2.

We also report the number of cycles as a function of the moment amplitude (see Fig. 7). For the sake of concision, we here only report results for the AL approach and the AD method at a coarse resolution. The behavior for WT_1 is very similar to the one discussed in Section 3 and will not be commented here. In simulations with CPC, compared to WT_1, WT_2 presents a different behavior. The peak related to the blade passage in the wind shear seems less marked, which is due to several reasons: first of all, the presence of the upstream wake increases the small scales of turbulence and this is translated by an increase of the cycle number in moments of small amplitude and a peak that appears less sharp in moments of medium amplitude. Second, the wake may also slightly mitigate the wind shear, slightly attenuating the peak observed in WT_1.

It is out of the scope of the present study but results of Fig. 7 do not translate an important increase of the fatigue damage for the second rotor in the line. Indeed, the number of cycles for the moments of large amplitude does not increase for WT_2, even though it is something that is usually observed in such a configuration and explained by the upstream wake meandering. Further investigations should be performed to explain this behavior (a wake meandering that is less marked due the simplicity of the rotor environment representation (synthetic turbulence boxes, etc) or a wake deficit that is less important than expected).

Figure 7 also highlights the effect of the CT-IPC for WT_2, with an impact of CT-IPC that is clearly less significant than for WT_1. It also shows that, for each rotor and control case, the AD and the AL approaches produce very similar cycle distributions.

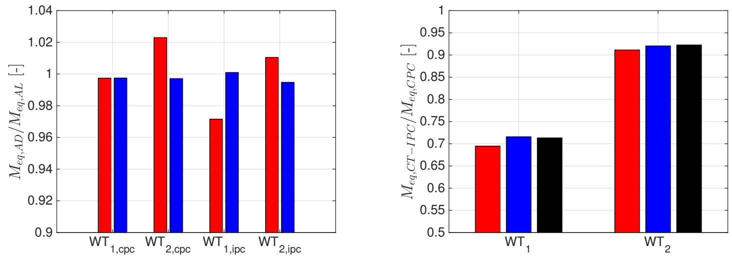

(a) $M_{eq,AD}/M_{eq,AL}$ (b) $M_{eq,CT-IPC}/M_{eq,CPC}$

Figure 6. Right: Ratio of the flapwise equivalent moment obtained using the AD method over the obtained using the AL approach (AD at a coarse resolution: red bars; AD at a finer resolution: blue bars). Left: Ratio of the flapwise equivalent moments obtained using CPC and CT-IPC, for the AD methods at a coarse resolution (red line) and at a fine resolution (blue line) and the AL approach (black line).

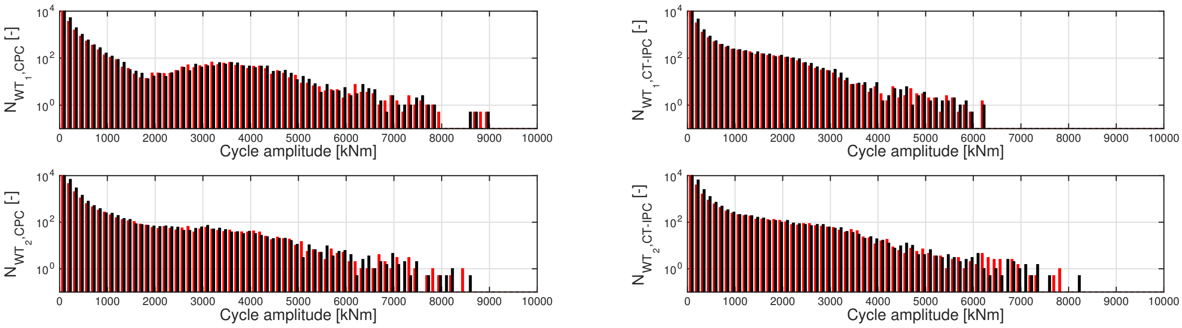

Figure 7. Number of cycles for M_f for the AD method at a coarse resolution (red bars) and the AL approach (black blars).

5. Conclusions

The present study aimed at assessing the Actuator Disk (AD) method supplemented with an Individual Pitch Control (IPC) strategy, at a resolution appropriate for the Large Eddy Simulation of large wind farms. The IPC scheme was based on a state-of-the-art individual pitch control [3], generalized to be applied to an AD approach. This procedure also required an accurate recovery of the flapwise bending moment on each blade, which is not trivial for a disk-type model and we based our approach on the methodology presented in Moens *et al.* [10]. We first assessed the IPC within the AD framework in simulations of an isolated wind turbine, for different wind speeds and turbulence intensities. The inflow consisted in a prescribed shear, over which turbulence fluctuations generated using the Mann algorithm [24] were imposed. We compared the AD statistics with those obtained using a discrete-type line approach, i.e. a state-of-the-art Actuator Line (AL) method. The comparison was mostly performed in terms of equivalent moment, a quantitative fatigue indicator. Globally, the results are close to each other, while we highlighted that simulations with more turbulence realizations or longer wind periods should decrease several of the observed differences. We then compared the AD method to the AL approach in a configuration with two rotors: again the results were very similar in both approaches (less than 3% of differences), even closer than those obtained in simulations with one rotor. Indeed, for this set of simulations, we performed three turbulence realizations (with the same turbulence intensity), over which the statistics were computed, allowing a better capture of the loading cycles of large amplitude, and a more consistent equivalent moment computation. This first study showed promising results and gave us confidence in deploying IPC strategies within an AD framework. However, this approach should be first verified in more complex environments (with a realistic Atmospheric Boundary Layer (ABL) representation, in a wind farm with more than two machines, etc) and with other IPC schemes [29].

Acknowledgments
This project has received funding from the European Research Council (ERC) under the European Union's Horizon 2020 research and innovation program (grant agreement no. 725627). Simulations were performed using computational resources provided by the Consortium des Équipements de Calcul Intensif (CÉCI), funded by the Fonds de la Recherche Scientifique de Belgique (F.R.S.-FNRS) under Grant No. 2.5020.11, and computational resources made available on the Tier-1 supercomputer of the Fédération Wallonie-Bruxelles, infrastructure funded by the Walloon Region under the Grant Agreement No. 1117545.

References

[1] Leithead W, Neilson V and Dominguez S 2009
[2] Zhang D, Cross P, Ma X and Li W 2013 Sensors and Actuators A: Physical **198** 8–14
[3] Bossanyi E A 2003 Wind Energy **6** 119–128
[4] Lio W H, Jones B L, Lu Q and Rossiter J A 2017 International Journal of Control **90** 37–52
[5] Frederik J A, Doekemeijer B M, Mulders S P and van Wingerden J W 2020 Wind Energy **23** 1739–1751
[6] Coquelet M, Bricteux L, Moens M and Chatelain P 2022 A reinforcement-learning approach for individual pitch control submitted for publication in Wind Energy
[7] Martínez-Tossas L and Leonardi S 2013 Wind turbine modeling for computational fluid dynamics Tech. Rep. SR-5000-55054 NREL
[8] Wu Y T and Porté-Agel F 2015 Renewable Energy **75** 945–955 ISSN 0960-1481
[9] Moens M, Duponcheel M, Winckelmans G and Chatelain P 2018 Wind Energy **21** 766–782
[10] Moens M, Duponcheel M and Chatelain P 2022 Assessment of an actuator disk-based approach for the prediction of fatigue loads in wind turbine rotors accepted with minor revisions, for publication in Wind Energy
[11] Duponcheel M, Bricteux L, Manconi M, Winckelmans G and Bartosiewicz Y 2014 International Journal of Heat and Mass Transfer **75** 470–482 ISSN 0017-9310
[12] Sørensen J N, Mikkelsen R F, Henningson D S, Ivanell S, Sarmast S and Andersen S J 2015 Phil. Trans. R. Soc. A **373** 20140071
[13] Trigaux F, Moens M, Chatelain P and Winckelmans G 2020 Journal of Physics: Conference Series **1618** 062035
[14] Wu Y T and Porté-Agel F 2011 Boundary-layer meteorology **138** 345–366
[15] Sarlak H, Meneveau C and Sorensen J 2015 Renewable Energy **77** 386–399 ISSN 0960-1481 URL `https://www.sciencedirect.com/science/article/pii/S0960148114008635`
[16] Churchfield M J, Lee S, Schmitz S and Wang Z 2015 33rd Wind Energy Symposium p 0214
[17] Stevens R J, Martínez-Tossas L A and Meneveau C 2018 Renewable Energy **116** 470–478
[18] Santoni C, Carrasquillo K, Arenas-Navarro I and Leonardi S 2017 Wind Energy **20** 1927–1939
[19] Bak C, Aagaard Madsen H and Johansen J 2001 Wind energy for the new millennium. Proceedings ed Helm P and Zervos A (WIP - Renewable Energies) pp 394–397 ISBN 88-900442-9-2
[20] Selvam K, Kanev S, van Wingerden J W, van Engelen T and Verhaegen M 2009 International Journal of Robust and Nonlinear Control: IFAC-Affiliated Journal **19** 72–91
[21] Lu Q, Bowyer R and Jones B L 2015 Wind Energy **18** 1451–1468
[22] Mulders S P, Pamososuryo A K, Disario G E and Wingerden J W v 2019 Wind Energy **22** 341–359
[23] Jonkman J, Butterfield S, Musial W and Scott G 2009 Definition of a 5-MW Reference Wind Turbine for Offshore System Development Tech. Rep. TP-500-38060 NREL
[24] Mann J 1998 Probabilistic Engineering Mechanics **13** 269 – 282 ISSN 0266-8920
[25] ASTM A E 2003 West Conshohocken (PA)
[26] Miner M 1945 Journal of Applied Mechanics **67** A159–A164
[27] Mandell J F and Samborsky D D 1997 DOE/MSU composite material fatigue database: test methods, materials, and analysis (Sandia National Laboratories Albuquerque)
[28] Ragan P and Manuel L 2007 Wind engineering **31** 83–99
[29] Coquelet M, Bricteux L, Lejeune M and Chatelain P 2020 Journal of Physics: Conference Series **1618** 022052